Spectroscopy of Hydrothermal Reactions. 8. Kinetics of Aqueous NH_4XCN (X = O, S) and OCS by Flow Reactor−Infrared Spectroscopy

P. G. Maiella and T. B. Brill*

Department of Chemistry and Biochemistry, University of Delaware, Newark, Delaware 19716

Received June 12, 1997

The kinetics and pathway of hydrothermolysis of 1 m NH_4SCN to CO_2, NH_3, and H_2S were determined at 543−573 K and 275 bar by the use of FTIR spectroscopy and a Pt/Ir flow reactor with diamond windows or a 316 stainless steel flow reactor with sapphire windows. The rates of SCN^- loss and CO_2 formation were the same. The reaction is (pseudo) second-order with $E_a = 113 \pm 11$ kg/mol and $\ln(A, \text{kg/(mol·s)}) = 21 \pm 2$. $\Delta S^{\ddagger} = -84$ J/(mol·K), which suggests a bimolecular, rate-determining, initial decomposition step for NH_4SCN. A reaction scheme is proposed in which OCS and a monothiocarbamate species are undetected intermediates. The absence of OCS is explained by the rapid hydrothermolysis rate of OCS to CO_2 and H_2S which was determined by IR spectroscopy at 393−423 K under 275 bar to be $E_a = 44 \pm 5$ kJ/mol and $\ln(A/s) = 13 \pm 1$ for OCS. The resulting rate is about 10^3 times faster than the hydrothermolysis rate of NH_4SCN at 543 K. The results are compared to the equivalent reaction for NH_4OCN. NH_4OCN reacts about 3×10^3 times faster than NH_4SCN at 543 K. The trend in the rates is consistent with the charge distribution and the trend in the bond distances, which resulted from *ab initio* quantum mechanical calculations at the HF/N311G//HF/N31G level in the OCN^- and SCN^- ions and the proposed carbamate and monothiocarbamate intermediates.

Introduction

Although the sulfur−carbon bond is fundamentally important in numerous areas, investigations of the hydrothermolysis of organosulfur compounds have been mostly motivated by practical issues. One of these issues is the destruction of organosulfur compounds in aqueous waste streams by hydrolysis and oxidation at high temperatures and pressures. Another issue is the desulfurization of biomass materials. Two process technologies that employ the reactivity of H_2O at high pressure and temperature are wet air oxidation,[1] where temperatures of 400−600 K and pressures of 5−200 bar are used, and supercritical water oxidation (SCWO),[2] where temperatures above 675 K and pressures above 250 bar are used. The critical point of water is 647 K and 221 bar.

The kinetics and mechanisms of hydrolysis of sulfur-containing chemical warfare agents in the normal liquid range of H_2O have been reviewed.[3] The kinetics of removal and/or the destruction efficiency of organosulfur compounds in the presence of H_2O at high pressure and temperature have been determined by applying wet air oxidation conditions to steel mill[4,5] and pulp mill[6] wastes, pesticides,[7] and coal.[8−10] The destruction efficiencies of smoke and dye compositions,[11] and of DMSO and mercaptans[2] are known at SCWO conditions. Mechanism studies of hydrothermolysis of organosulfur compounds have been reported,[12,13] and bond homolysis mechanisms in sulfur mustard have been explored with *ab initio* Gaussian 92 calculations in a "solvent" field of various dielectric constants including those at hydrothermal conditions.[14]

Most previous hydrothermal studies are based on batch reaction methods with *ex situ* determination of the products. In light of the ubiquity of compounds containing the S−C bond in natural and industrial products, we sought to determine the kinetics and mechanism of hydrothermolysis of such a bond by direct spectroscopic measurements. The thiocyanate ion, SCN^-, was chosen for study (as the NH_4^+ salt) for several reasons. First, from the practical point of view the SCN^- ion is present in coke oven gas wastewater[3,4] and is considered to be non-biodegradable.[15] Therefore, the kinetics and mechanism of hydrothermolysis have potentially immediate consequences as a destruction method. Second, the intense absorbance of $\nu_3(SCN^-)$ in the mid-IR provides an easy probe of its concentration in an IR flow cell. Third, SCN^- is not expected to

* Correspondence author.

(1) Mishra, V. S.; Mahajani, V. V.; Joshi, J. B. *Ind. Eng. Chem. Res.* **1995**, *34*, 2.
(2) Tester, J. W.; Holgate, H. R.; Armellini, F. J.; Webley, P. A.; Killilea, W. R.; Hong, G. T.; Barner, H. E. In *Emerging Technologies in Hazardous Waste Management III*; ACS Symposium Series 518, Tedder, D. W., Pohland, F. G., Eds.; American Chemical Society: Washington, DC, 1993; p 35.
(3) Yang, Y.-C.; Baker, J. A.; Ward, J. R. *Chem. Rev.* **1992**, *92*, 1729.
(4) Chowdhury, A. K.; Copa, W. C. *Ind. Chem. Eng.* **1986**, *28*, 3.
(5) Copa, W. M.; Gitchel, W. B. *Standard Handbook of Hazardous Waste Treatment and Disposal*; Freeman, H. M., Ed.; McGraw-Hill: New York, 1989; Sec. 8.8.
(6) Schoeffel, E. W.; Seegert, N. *Wasser, Luft Betr.* **1966**, *8*, 541; *Chem. Abstr.* **1966**, *65*, 18317.
(7) Randall, T. L. *Industrial Waste, Proceedings of the 13th Mid-Atlantic Conference*; Huang, C. P., Ed.; Ann Arbor Science Publishers: Ann Arbor, MI, 1981; p 501.
(8) Slagle, D.; Shah, Y. T.; Joshi, J. B.; Brainard, A. J. *Ind. Eng. Proc. Res. Dev.* **1980**, *19*, 294.
(9) Lagonik, F. E.; Shah, Y. T.; Albal, R. S.; Joshi, J. B.; Brainard, A. J. *Chem. Eng. Commun.* **1981**, *11*, 201.
(10) Joshi, J. B.; Shah, Y. T. *Fuel* **1981**, *60*, 612.
(11) Rice, S. F.; LaJeunesse, C. A.; Hanush, R. G.; Aiken, J. D.; Johnston, S. C. *SAND94−8209*, Sandia National Laboratories: Livermore, CA, Jan 1994.
(12) Abraham, M. A.; Klein, M. T. *Fuel Sci. Tech. Int.* **1988**, *6*, 633.
(13) Katritzky, A. R.; Lapucha, A. R.; Greenhill, J. V.; Siskin, M. *Energy Fuels* **1990**, *4*, 562−571. Katritzky, A. R.; Lapucha, A. R.; Luxam, F. J.; Greenhill, J. V.; Siskin, M. *Energy Fuels* **1990**, 4, 572−577. Katritzky, A. R.; Murugan, R.; Siskin, M. *Energy Fuels* **1990**, *4*, 577.
(14) Politzer, P.; Habibollahzadeh, D. *J. Phys. Chem.* **1994**, *98*, 1576.
(15) Horak, O. *Chem. Ing. Tech.* **1990**, *6*, 555.

S0020-1669(97)00723-4 CCC: $15.00
Published on Web 01/22/1998

produce a precipitate or other deleterious products that are incompatible with a micro flow reactor. Fourth, kinetic data for hydrothermolysis of the congener salt, NH_4OCN, have recently been determined by the same IR spectroscopic method,[16,17] so that the hydrothermolysis rates of NH_4SCN and NH_4OCN can be directly compared for the first time.

It is reasonable that the reactions studied here might be catalyzed by acid and/or base. By the determination of the hydrothermolysis kinetics of the salt in water mostly in the absence of added acid or base, the lower limit of the reaction rate is revealed, which has practical value in the degradation process.

Experimental Section

The 90/10 Pt/Ir-diamond flow cell[16] and the 316 SS-sapphire cell[17] function as the reactor as well as the observation port in the system. They are transmission IR spectroscopy cells having a path length (30 $\pm$ 5 μm) that is controlled by the thickness of an Au-foil washer. The exact path length ($\pm$1 μm) was determined by the interference fringe spacing in the IR spectrum. No detectable change in the path length was observed at the different conditions used. The heat transfer and fluid mechanics characteristics of these cells have been determined,[16] so that the temperature profiles and flow patterns are known. Plug flow conditions can be assumed at the higher flow rates (lower degree of conversion); however, laminar flow is a better description at lower flow rates.

The flow controls for the cells were described previously.[17] Briefly, the flow rate was controlled with an accuracy of $\pm$0.01 mL/min by the output of a pulseless LDC-Analytical, dual-piston, HPLC pump. The flow rate was monitored continuously by an Intek-Rheotherm calorimetric flow meter. The temperature was maintained in the (543−593) $\pm$ 1 K range by electrical cartridge heaters mounted concentrically in the cell block. Active control of these heaters was achieved with Omega PID control units connected to 0.8 mm K-type thermocouples mounted in the cell block near the fluid path. The pressure was maintained at 275 $\pm$ 1 bar by an air-actuated bleed-and-lock valve system. The pressure was activity monitored with an Omega melt pressure transducer. Software written in Visual Basic was used to control and record the temperature, pressure, and flow rate at all times. IR spectra were taken only after the system had stabilized at each set of conditions.

A 1.00 m (mol/kg) solution of NH_4SCN (Aldrich) was prepared by dissolving the colorless crystals in HPLC-grade H_2O that had been sparged with Ar for 30 min to remove dissolved atmospheric gases. The hydrothermolysis reaction was characterized in 10 K intervals over 543−573 K using about 15 different flow rates at each temperature. Flow rates of 1.25−0.05 mL/min yielded residence times in the cell of 2.5−49 s. At each set of conditions, 32 interferograms were summed at 4 cm^{-1} resolution using a Nicolet 60 SX FTIR spectrometer employing a liquid N_2-cooled MCT detector. Each spectrum was ratioed against the spectrum of pure H_2O at the same pressure and temperature to remove as much of the absorbance by H_2O as possible. The spectral features revealed the existence of a single (liquid) phase at all of the conditions used. Figure 1 illustrates several spectra that are discussed in this article.

Conversion of the spectral absorbance areas into concentrations required acquisition of calibration data based on the Lambert−Beer law. $\nu_3(CO_2)$ for the CO_2-H_2O system has been characterized for this purpose in the infrared region,[17] but adjustment of the absorbance values of CO_2 to match the required carbon balance at the end of the reaction corrects for small variations in the volume of the different cells and differences in the cell alignment.[18] The spectral band areas were then determined by using curve fitting software (Peakfit, Jandel Scientific) with a four-parameter Voigt function. These areas were converted to concentrations by using the calibration data and were corrected for the change in density of H_2O [0.795 g/cm^3 (543 K) to 0.747 g/cm^3 (573 K)].

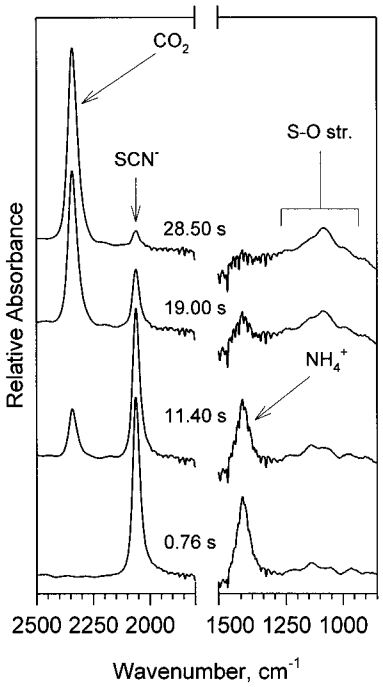

Figure 1. Mid-IR spectra of 1.00 m NH_4SCN at 275 bar and 593 K at several residence times in the Pt/Ir-diamond window flow cell.

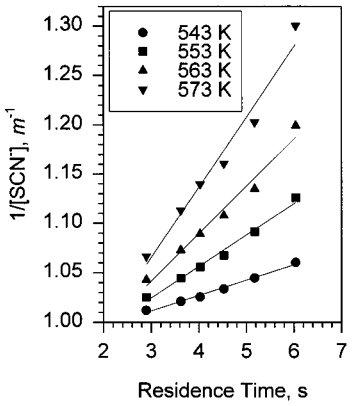

Figure 2. Pseudo-second-order rate plots for the disappearance of SCN^- in 1.00 m NH_4SCN at 275 bar (Table 1).

Table 1. Pseudo-Second-Order Rate Constants for Hydrothermolysis of NH_4SCN (CO_2 Formation at 275 bar)

T, K	*k*, kg/(mol·s)	*T*, K	*k*, kg/(mol·s)
543	0.022 $\pm$ 0.009	563	0.046 $\pm$ 0.004
553	0.027 $\pm$ 0.004	573	0.066 $\pm$ 0.006

The reaction was determined to have a second-order rate law on the basis of the linear plot of 1/[SCN^-] vs time (Figure 2). The concentration of SCN^- was determined from the IR absorbance and also by the carbon mass balance based on the rate of formation of CO_2. Both gave the same rate within the uncertainty of the experiment. The CO_2 data were used because we have experience with the CO_2 line shape and absorptivity in H_2O up to 350 °C.[17,18] Table 1 contains the resulting rate constants.

The reaction was determined to be first order with respect to NH_4^+ and SCN^- by adding known concentrations of NH_4NO_3 to vary the NH_4^+ concentration and KSCN to vary the SCN^- concentration. These solutions were run in triplicate at 553 K and 275 bar for 13 residence times. This temperature is below the decomposition temperature of aqueous NH_4NO_3 in our flow cell.[16] Table 2 contains the observed

(16) Schoppelrei, J. W.; Kieke, M. L.; Wang, X.; Klein, M. T.; Brill, T. B. *J. Phys. Chem.* **1996**, *100*, 14343.
(17) Kieke, M. L.; Schoppelrei, J. W.; Brill, T. B. *J. Phys. Chem.* **1996**, *100*, 7455.
(18) Maiella, P. G.; Brill, T. B. Unpublished results.

Table 2. Effect on the Rate of CO_2 Formation of Excess NH_4^+ and SCN^- in 1.0 m NH_4SCN ($T = 553$ K, $P = 275$ bar)

concn. kg/mol				
NH_4SCN	NH_4NO_3	KSCN	k_{obsd}, kg/(mol·s)	k_{obsd}/[X]
1.0	0	0	0.027 ± 0.004	0.027
1.0	0.5	0	0.038 ± 0.005	0.025
1.0	0.75	0	0.046 ± 0.007	0.026
1.0	1.0	0	0.050 ± 0.005	0.025
1.0	0	0.5	0.043 ± 0.009	0.029
1.0	0	0.75	0.049 ± 0.003	0.028
1.0	0	1.0	0.055 ± 0.008	0.028

rate constants calculated from the appropriate rate expression[19] when excess NH_4^+ and excess SCN^- have been added. The kinetic analysis was limited to residence times of 10 s or less so that plug flow conditions could be assumed. Weighted least-squares regressions were used to determine all of the rate constants and Arrhenius parameters. The statistical weight ω_i used was $1/\sigma^2$, where σ is the standard deviation. Where applicable, ω_i was approximated as $k^2\omega_i$.[20]

The products of hydrothermolysis of NH_4SCN were also identified after heating the solution in a sealed 12 cm^3 316 SS tube in a fluidized sand bath. By the trapping of the gases released when the tube was opened, the existence of H_2S, which was not detected in the IR spectrum due to its low molar absorptivity, was confirmed by its mass spectrum ($m/z = 32, 33, 34$).

The kinetics of hydrothermolysis of carbonyl sulfide were determined on an aqueous solution that had been saturated with OCS (Matheson) by bubbling and stirring in an autoclave for approximately 175 min at 296 K. The solutions had a concentration of approximately 0.25 m based on total conversion to CO_2. This solution was pumped in the closed flow reactor as described above, and the rate of conversion to CO_2 was measured at 393−423 K under 275 bar.

We had hoped to include the hydrothermolysis of NH_4SeCN in this study for comparison with NH_4OCN and NH_4SCN. NH_4SeCN was synthesized,[21] but the plan was abandoned when it was found by batch reaction that Se deposited on the tube walls. Such an occurrence would plug the flow reactor. Although the mechanism of hydrothermolysis of NH_4SeCN was not determined, the formation of solid Se may result from the $H_2Se \rightleftharpoons H_2 + Se$ equilibrium.

Ab initio quantum mechanical calculations were performed with the General Atomic and Molecular Electronic Structure System (GAMESS).[22] The energy gradient method was used to optimize the geometry of each species. Urea, carbamate, and cyanate were optimized by using the HF/311G basis set. The HF/31G basis set was used for thiourea, monothiocarbamate, and thiocyanate. Vibrational frequencies were calculated using second derivatives at the forementioned levels to confirm the stationary point structures. Second-order Møller−Plesset perturbation calculations (MP2)[23,24] at the forementioned levels were executed to account for the effects of electron correlation in the total energies.

Results and Discussion

Ammonium Cyanate Data. The kinetics of hydrothermolysis of NH_4OCN have been determined by IR spectroscopy in the same Pt/Ir-diamond and 316 SS-sapphire cells as were used to investigate NH_4SCN.[16,17] It was not feasible, however, to determine the hydrothermolysis kinetics of NH_4OCN directly by simply dissolving the salt in H_2O, because it decomposed rapidly in the temperature range of interest. Instead, the kinetics were acquired by modeling the hydrothermolysis of 1.05 m urea at 473−573 K in which the hydrothermolysis of NH_4OCN is one of the observable steps. The most consistent rate constants and Arrhenius parameters were extracted from the species profiles of eqs 1 and 2 by using the appropriate, iteratively-solved, differential rate expressions.[16,17] Table 3 gives the Arrhenius parameters for the pseudo-second-order eq 2 determined with cells constructed from two different materials. The differences in the NH_4OCN data can be attributed to error in the assumed cell volume and/or, possibly, to a small contribution from the difference in the materials of construction.

Table 3. Arrhenius Parameters in H_2O at 275 bar

reacn	cell	T, K	E_a, kJ/mol	ln(A, kg/(mol·s))
NH_4OCN (eq 2)	Pt/Ir-diamond	473−573	67.5 ± 7	18.6 ± 0.3
NH_4OCN (eq 2)	316 SS-sapphire	473−573	59	17.1
NH_4SCN (eq 3)	316 SS-sapphire	543−573	113 ± 11	21 ± 2
OCS (eq 7)	316 SS-sapphire	393−423	44 ± 5	13 ± 1[a]

[a] Units are s^{-1}.

$$(NH_2)_2CO \rightarrow NH_4^+ + OCN^- \quad (1)$$

$$NH_4^+ + OCN^- (+H_2O) \rightarrow CO_2 + 2NH_3 \quad (2)$$

Ammonium Thiocyanate Spectra and Kinetics. Unlike NH_4OCN, the hydrothermolysis reaction of 1.00 m NH_4SCN could be followed directly in both the 316 SS-sapphire cell and the Pt/Ir-diamond cell at a constant pressure of 275 bar as a function of temperature and flow rate. This was possible because NH_4SCN reacted more slowly than NH_4OCN. The temperature range used for kinetics was 543−573 K, although data were collected up to 593 K. Figure 1 shows spectra selected from experiments with the Pt/Ir-diamond cell. Absorbances for the SCN^- and NH_4^+ reactant ions are clearly apparent at short residence times in which the reaction is at an early stage. They diminish in intensity at longer residence times and are replaced by the absorbance of aqueous CO_2. Apart from the appearance of a broad, weak absorbance centered at about 1100 cm^{-1} at the highest temperature used, no other products are apparent. Although the exact origin of this latter absorbance is unknown at this time, it appears in the intensely IR-active S−O stretching region. This suggests that oxidation of the H_2S product occurs. The amount of oxidation is apparently small because the intensity is relatively low. Extensive oxidation of sulfur is known to occur when an $S-H_2O$ mixture is held at 638 K in the batch mode for longer times.[25]

Studies in which the concentrations of NH_4^+ and SCN^- were independently varied showed that the rate of hydrothermolysis of NH_4SCN was essentially first-order in NH_4^+ and in SCN^- (Table 2). Thus, the rate should be second-order in NH_4SCN, which is consistent with eq 3 and was validated by plotting

$$NH_4^+ + SCN^- + 2H_2O \rightarrow CO_2 + 2NH_3 + H_2S \quad (3)$$

$1/(C_0 - [CO_2])$ vs the residence time as shown in Figure 2. Because of the probable role of H_2O in the reaction, these rates (Table 1) are best described as pseudo-second-order. A plot of the rate constants at 543−573 K yields the Arrhenius plot shown in Figure 3 and Arrhenius parameters shown in Table 3. Also shown in Figure 3 is the equivalent Arrhenius plot for NH_4-

(19) Connors, K. A. *Chemical Kinetics*; VCH Publ. Inc.: New York, 1990.
(20) Cvetanovic, R. J.; Singleton, D. L. *Int. J. Chem. Kinet.* **1977**, *9*, 481.
(21) Geisler, K.; Nobst, E.; Müller, C.; Bulka, E. *Z. Chem.* **1982**, *22*, 113.
(22) Schmidt, M. W.; Baldridge, K. K.; Boarz, J. A.; Elbert, S. T.; Gordon, M. S.; Jensen, J. H.; Koseki, S.; Matsunaga, N.; Nguyen, K. A.; Su, S. J.; Windus, T. L.; Dupuis, M.; Montgomery, J. A. *J. Comput. Chem.* **1993**, *14*, 1347.
(23) Binkley, J. S.; Pople, J. A.; Hehre, W. J. *J. Am. Chem. Soc.* **1975**, *97*, 229.
(24) Pople, J. A.; Hehre, W. J. *Int. J. Quantum Chem. Symp.* **1976**, *10*, 1.
(25) Sorokin, V. I.; Orlov, R. Yu.; Dadze, T. P. *Proceedings of the First International Conference on Solvo-thermal Reactions*; Shikoku National Industrial Research Institute: Takamatsu, Japan, Dec. 1994; paper S-5.

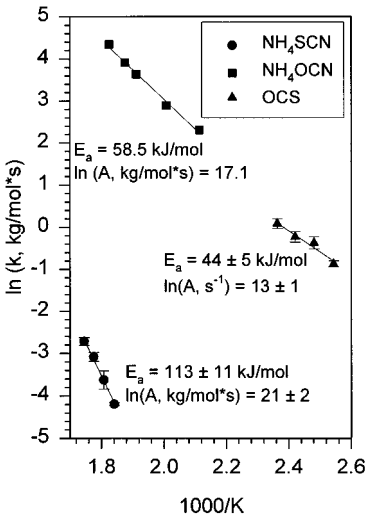

Figure 3. Arrhenius plots for decomposition of aqueous NH_4SCN, NH_4OCN, and OCS at 275 bar.

OCN for comparison with NH_4SCN. It is obvious that the rate of hydrolysis of NH_4SCN is slower than that of NH_4OCN under the same conditions.

An indication of the molecularity of these reactions is provided by $\Delta S^{\ddagger}$. At 543 K in the 316 SS-sapphire cell, $\Delta S^{\ddagger} = -113$ J/(mol·K) for NH_4OCN and -84 J/(mol·K) for NH_4SCN. These values compare well to the approximate range for bimolecular reactions (~ -63 to -125 J/(mol·K)),[19] which is consistent with the pseudo-second-order rate expression determined for eqs 2 and 3. The more negative value of $\Delta S^{\ddagger}$ for NH_4OCN is consistent with the greater charge compactness of the OCN^- ion compared to SCN^-, which enhances the electrostriction of the surrounding H_2O field.

Reaction Pathways. Based on the spectra in Figure 1, eqs 4 and 5 are one potential pathway of hydrothermolysis of NH_4SCN

$$NH_4^+ + SCN^- + H_2O \rightarrow NH_4^+ + OCN^- + H_2S \quad (4)$$

$$NH_4^+ + OCN^- + H_2O \rightarrow CO_2 + 2NH_3 \quad (5)$$

SCN giving eq 3. This scheme was firmly rejected on the basis of the absence of the intensely active stretching mode of OCN^- at 2165 cm^{-1}. This mode is readily detectable in the 543 K temperature range when OCN^- is present at greater than 0.01 m.[16,17] On the other hand, the presence of H_2S was apparent by its pungent odor and was confirmed by mass spectrometry (*vide supra)*. Quantitation of H_2S by mass spectrometry was not satisfactory probably for the reasons that a two-phase system exists after depressurization and the fact that some of the H_2S is oxidized (Figure 1). H_2S(aq) was expected to be observed in the IR spectrum by ν(SH) at about 2680 cm^{-1}; however, in contrast to the O−H stretch of H_2O, the S−H stretch of H_2S has low intensity, in part because hydrogen bonding by H_2S is weak. No H_2S could be detected by IR spectroscopy even in an H_2O standard solution that had been saturated with H_2S.

A more justifiable pathway of hydrothermolysis of NH_4SCN is given by eqs 6 and 7. At first sight this scheme appears to

$$NH_4^+ + SCN^- + H_2O \rightarrow 2NH_3 + OCS \quad (6)$$

$$OCS + H_2O \rightarrow CO_2 + H_2S \quad (7)$$

be no more satisfactory than eqs 4 and 5 because the intensely IR-active ν_3(OCS) at about 2100 cm^{-1} is, like OCN^- in eq 4, absent. However, unlike OCN^- which should be detected if it is present,[16,17] the absence of OCS was understood after its kinetics of hydrothermolysis were determined as described next.

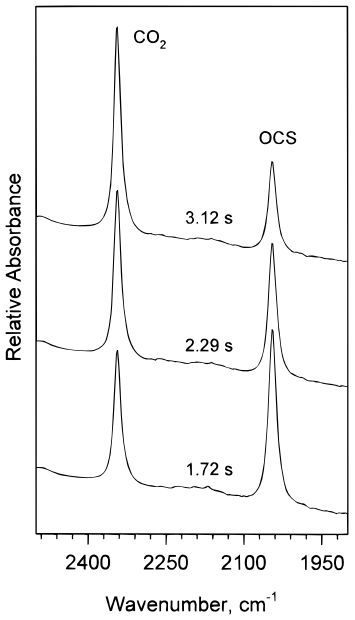

Figure 4. Mid-IR spectra of approximately 0.25 m OCS during hydrothermolysis at 493 K and 275 bar at several residence times in the 316 SS flow reactor.

Table 4. Pseudo-First-Order Rate Constants for Hydrothermolysis of OCS (CO_2 Formation at 275 bar)

T, K	*k*, (s^{-1})	*T*, K	*k*, (s^{-1})
393	0.42 ± 0.03	413	0.80 ± 0.10
403	0.70 ± 0.10	423	1.10 ± 0.12

Figure 4 shows IR spectra of the C−O stretching region of approximately 0.25 molal OCS during the conversion to CO_2 by eq 7 at 393 K under 275 bar. Several of many residence times recorded are shown. As with the NH_4SCN solution above, no H_2S could be detected, which is consistent with its low IR absorptivity. Conversion of the CO_2 areas into concentrations provides the pseudo-first-order rate constants for eq 7 at 393−423 K under 275 bar. These rate constants are given in Table 4 and provide the Arrhenius plot shown in Figure 3. The comparatively low activation energy of 44 ± 5 kJ/mol (Table 3) makes the reaction facile despite the fact that the *A* factor suggests at least bimolecular character ($\Delta S^{\ddagger} = -150$ J/(mol·K)). Bimolecularity is not inconsistent with a pseudo-first-order rate expression for eq 7. Extrapolation of the rate of hydrothermolysis of OCS to 543 K, where the slowest rate of decomposition of NH_4SCN was measured, indicates that OCS decomposes about 10^3 times faster than NH_4SCN. Consequently, the OCS concentration will be below the limit of detection in our cell. As a result of these findings, the net hydrothermolysis reaction for NH_4SCN (eq 3), which parallels eq 2 for NH_4OCN, is proposed to be the result of eqs 6 and 7.

The rate differences found are helpful for hypothesizing further details about the pathway of eqs 2 and 3. Figure 5 shows the proposed scheme. For comparison, the rate constants at 543 K are shown as derived from the Arrhenius data in Table 3. Hydrothermolysis of NH_4SCN and NH_4OCN plausibly begins with association of H_2O and the electropositive carbon atom of the ion pair. Incidently, ion-pair formation by salts is increasingly favored in water at higher temperatures because the bulk dielectric constant of water decreases with increasing

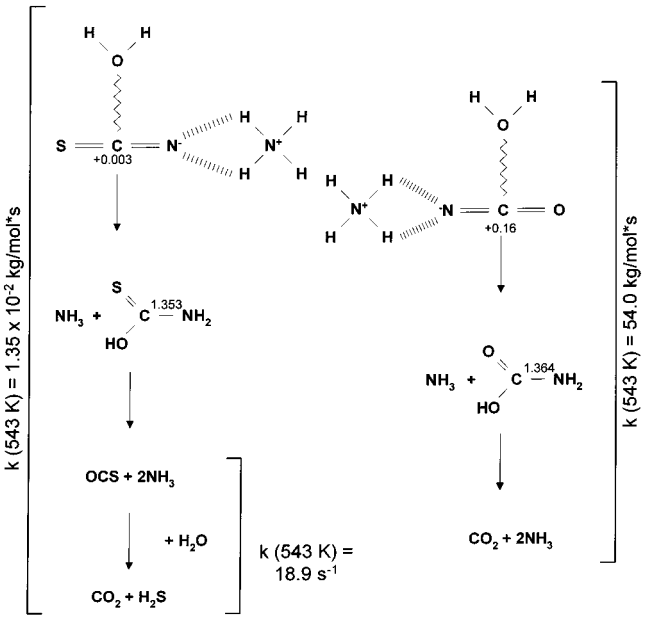

Figure 5. Proposed hydrothermolysis pathway for aqueous NH_4SCN and NH_4OCN showing charges and bond parameters (Å) from *ab initio* quantum mechanical calculations and rate comparisons at 543 K under 275 bar.

temperature.[26] Many possible ways now exist for migration of hydrogen as a C−O bond forms. The rate of reaction is, however, expected to be slower for SCN^- because a Mulliken population analysis indicates that less positive charge resides on the carbon atom in SCN^- (+0.003) than OCN^- (+0.159). Hence, the initial $H_2O\cdots C$ interaction is weaker in SCN^-. Reasonable resulting intermediates of hydrolysis of NH_4OCN and NH_4SCN are the carbamic and the monothiocarbamic acids or their anions, respectively, along with NH_3 (Figure 5). However, the steady-state concentrations of the carbamate and monothiocarbamate species are expected to be below the limit of detection at the temperature of this study. This expectation is based on the fact that, although the carbamate ion can be detected at as high as 450 K in the Raman spectrum of aqueous $(NH_4)_2CO_3$,[27] it is not detected at this temperature by IR spectroscopy.[17]

The rate of conversion of the monothiocarbamate species to OCS and NH_3 in Figure 5 is expected to be slower than the carbamate species. This is a consequence of the *ab initio* quantum mechanical calculations on $NH_2C(O)OH$ and $NH_2C(S)OH$ that reveal the C−N bond to be shorter in the latter compound. The same trend is also found in calculations on the anions (1.42 and 1.46 Å, respectively). We emphasize, however, that the rate-controlling step of hydrothermolysis of NH_4SCN is proposed to be the initial pseudo-second-order step but suggest that the second step in Figure 5, which includes breaking of the C−N bond, may also be slower when S is bound to C than when O is bound to C.

Because NH_4^+ acts as a proton donor in the initial step of Figure 5, an increase in the pH should decrease the rate. A KOH solution was added to 1.00 m NH_4SCN to raise the pH to 11.25 (at 295 K). The rate constant of hydrothermolysis of NH_4SCN at 543 K was observed to be $2.2 \pm 0.2 \times 10^{-3}$ kg/(mol.s), which is one-tenth the value for the 1.00 m NH_4SCN solution (Table 1). No reaction at all was detected at 543 K when the pH was raised to 14. To conclude discussion of Figure 5, the absence of OCS in the IR spectrum during the hydrothermolysis of NH_4SCN was explained by the kinetics of hydrothermolysis of OCS described above. Its rate constant at 543 K is about 10^3 times faster than the hydrothermolysis rate of NH_4SCN at this temperature.

The comments just made suggested reasons that elimination of the C−N bond during hydrothermolysis of X−C−N linkages is impeded when X = S compared to X = O. This pattern also exists in compounds related to NH_4OCN and NH_4SCN, such as their compositional isomers urea, $(NH_2)_2CO$, and thiourea, $(NH_2)_2CS$. Each has two C−N bonds. The rearrangement of these compounds by eqs 8[28] and 9[29] is well-known.

$$(NH_2)_2CO \rightleftharpoons NH_4OCN \quad (8)$$

$$(NH_2)_2CS \rightleftharpoons NH_4SCN \quad (9)$$

The first-order kinetics of the forward reaction in eq 8 in H_2O have been determined at 333−363 K[30] and at 473−573 K.[16,17] Kinetics of the forward reaction of eq 9 in H_2O are known only at 363−403 K.[31] Thus, the rates of these reactions are most safely compared at 363 K, and the effect of X = S or O on scission of the first of two XC−N bonds is thereby indicated. For thiourea[31] $k = 1.5 \times 10^{14} \exp(-18.06/T)\ s^{-1}$. For urea[30] $k = 3.8 \times 10^{14} \exp(-16.37/T)\ s^{-1}$. The rate of conversion of thiourea is, therefore, about 250 times slower than urea at 363 K implying, as before, that S impedes the scission of the C−N bonds in these compounds more than O. In keeping with the kinetics, the average C−N bond distance in $(NH_2)_2CS$ is shorter [1.33 Å (X-ray[32]), 1.37 Å (calcd)] than that in $(NH_2)_2CO$ [1.34 Å (X-ray[33]), 1.39 Å (calcd)]. The calculated values were obtained by the *ab initio* quantum mechanical calculations described above.

In summary, the first spectroscopic measurements were made on the decomposition of compounds containing the XCN linkage (X = O, S) in the neutral hydrothermal medium. Kinetic constants reveal that the rate of the reaction is slower when X = S. While not directly successful in revealing the intermediates, the IR spectra provide the basis for rationally sorting out the pathways. The coupling of *in situ* spectral data and *ab initio* quantum mechanical calculations provides reasonable insight into the mechanism under demanding experimental conditions.

Acknowledgment. We are grateful to the U. S. Army Research office for support of this work on Grant DAAL03-92-G-0174. We thank Steven D. Bennett for help with the computational methods.

IC970723S

(26) Uematsu, M.; Franck, E. U. *Phys. Chem. Ref. Data* **1980**, *9*, 1291.
(27) Schoppelrei, J. W.; Kieke, M. L.; Brill, T. B. *J. Phys. Chem.* **1996**, *100*, 7463.
(28) Wöhler, F. *Pogg. Ann.* **1828**, *12*, 253.
(29) Reynolds, J. E. *J. Chem Soc.* **1869**, *22*, 1.
(30) Shaw, W. H. R.; Bordeaux, J. J. *J. Am. Chem. Soc.* **1955**, *77*, 4729.
(31) Shaw, W. H. R.; Walker, D. G. *J. Am. Chem. Soc.* **1956**, *78*, 5769.
(32) Kutoglu, A.; Scheringer, C.; Meyer, H.; Schweig, A. *Acta Crystallogr.* **1982**, *B38*, 2626.
(33) Mullen, D.; Hellner, E. *Acta Crystallogr.* **1978**, *B34*, 1624.